Dynamics of trace metal sorption by an ion-exchange chelating resin described by a mixed intraparticle/film diffusion transport model. The Cd/Chelex case.

F. Quattrini[a], J. Galceran[a] , C.A. David[a], J. Puy[a], G. Alberti[b], and C. Rey-Castro[a*]

[a]Departament de Química, Universitat de Lleida, Rovira Roure 191, 25198 Lleida, Catalonia, Spain

[b]Dipartimento di Chimica, Università degli Studi di Pavia, via Torquato Taramelli 12, 27100 Pavia, Italy

* corresponding author email: carlos.rey@quimica.udl.cat

Abstract

The time-evolution of Cd^{2+} ion sorption by Chelex 100 resin was studied in batch experiments as a function of time, pH, ionic strength, stirring rate, mass of resin and initial metal ion concentration. In the experimental conditions, the amount of resin sites are in excess with respect to the amount of metal ion, leading to extensive depletion of metal in bulk solution when equilibrium is reached. The data were described using a mixed control mass transport model in finite volume conditions (MCM) that includes explicitly both intraparticle and film diffusion steps. Exact numerical computations and a new approximate analytical expression of this model are reported here. MCM successfully predicts the influence of pH and ionic strength on the experimental Cd(II)/Chelex kinetic profiles (which cannot be justified by a pure film diffusion controlled mechanism) with a minimum number of fitting parameters. The overall diffusion coefficient inside the resin was modelled in terms of the Donnan factor and the resin/cation binding stability constant. The values of the latter coefficient as a function of pH and ionic strength were estimated from the Gibbs-Donnan model. Even though MCM is numerically more involved than models exclusively restricted to film or

intraparticle diffusion control, it proves to be accurate in a wider range of values of the mass transfer Biot number and solution/resin metal ratios.

Keywords: chelating resins, trace metals, particle diffusion control, film diffusion control, DGT passive sampler

1. Introduction

Chelating ion exchange resins (like Chelex100) have a number of advantageous features for the separation of metal ions in aqueous solution, like high selectivity and efficiency of binding, good physical and chemical stability, commercial availability in a wide range of particle sizes and porosities, etc. Consequently, this kind of resins has found numerous applications in different fields, such as DNA purification [1], removal of hazardous materials from wastewater [2, 3], recovery of precious metals from leachates [4], chemical speciation studies in environmental matrices [5-9], or extraction and pre-concentration of ions of analytical interest [10] for *e.g.* the determination of nanomaterial solubility [11].

One particularly successful application consists in the resin beads being embedded in a polymeric gel to obtain a metal-binding layer that is at the core of the DGT (Diffusive Gradients in Thin films) sampler, a widely used technique for the detection of trace elements and nutrients in natural waters, soils and sediments [12-16]. The study of the physicochemical mechanisms that regulate the metal accumulation is essential for the interpretation of the DGT performance in varying environmental conditions (pH, ionic strength, etc.) [17-20]. However, the mechanisms that govern the kinetics of metal uptake by the free resin beads need further study.

The use of chelating ion exchange resins for trace metal speciation and wastewater treatment is most often focused on systems characterized by low concentrations of the trace metal and excess concentration of background electrolyte. In these situations, the

uptake of the analyte takes place in the presence of large concentrations of the major counterions in both the resin and aqueous phases, which are typically unaffected by the ion-exchange process, so that the mutual ion diffusion coefficients remain constant [21]. The chemical reaction step between the metal ion of interest and the functional groups in the resin is typically very fast, so that the rate-controlling process is the diffusion of the trace ion. Moreover, in these dilute systems, the use of mass transport models rigorously derived for isotopic ion exchange can be safely extended to cases where a divalent trace ion is exchanged with a monovalent major counterion in excess, since inter-diffusion coefficients approach the value of the self-diffusion coefficient of the trace ion [22, 23]. As a result, models based on Fick's law can be used quite accurately, without the necessity of solving the Nernst-Planck equation.

The experimental study of the dynamic behaviour of these systems is often performed in isothermal conditions using stirred batch reactors, where the decay in the concentration of trace metal in bulk solution is monitored during the sorption process. Therefore, finite volume conditions apply, where partition ratios between moles of metal sorbed at equilibrium and total amount of metal are typically close to one. The equations for the corresponding models assuming internal diffusion in the gel particles or diffusion in the external liquid boundary layer, both in infinite or finite volume conditions, can be found in the classical monographies on ion exchange systems [2, 21, 22, 24-27]. Some of these models have been used in the recent literature on metal sorption by Chelex resins [28, 29], with some controversy on the relative roles of the intraparticle and external boundary film transport controlling mechanisms.

In particular, the model based on transport control by diffusion in the boundary solution layer was proposed (in infinite volume conditions) by Boyd [30], while the case of finite volume was reported later on [22] (see for instance, eqn. 4.63 in the work by

Inglezakis [21]). An outline of the concentration profiles at short times (when the surface can be considered as a perfect sink) is seen as inset of Fig 1. This model, denoted here as Film Diffusion Model (FDM), although showing good agreement with experimental kinetic data at relatively short fractional uptake values, has some limitations. As will be shown in the present work, experimental deviations from the FDM are observed at long times and, what is more important, the model does not provide a theoretical support for the observed influence of pH and ionic strength on the kinetic data. On the other hand, the model assuming the ion exchange process as controlled by internal diffusion in finite volume conditions was solved by Paterson [31] and used by others [22, 32, 33], and is here denoted as intraparticle diffusion model (IDM).This model has the obvious disadvantage of being unable to account for the observed effect of the stirring rate in batch experiments.

Although some authors have reported a transition from external film to intraparticle diffusion regimes during the kinetic experiments [34], examples of application of mixed-control diffusion models to ion exchange in bulk depletion conditions are still very scarce [35], and unprecedented in the particular case of trace metal ions. One reason for this gap may be the relative mathematical complexity of the available analytical solutions, which are expressed as infinite series (see references [36] and [27] for the cases of infinite and finite volume conditions).

Furthermore, while the thermodynamic description of pH and ionic strength effects on the metal/resin binding properties at equilibrium is well developed, there is still a need for the incorporation of such effects into consistent kinetic models beyond the *ad-hoc* introduction of additional empirical parameters (*e.g.*, conditional values of diffusion coefficients specifically fitted for each medium).

The purpose of the present work is to fill this gap, in three ways. First, it reports an approximate (but very accurate) analytical solution to the Mixed Control Model (MCM) for finite volume conditions, which compares favourably with the infinite series expression (16-112) listed by Le Van [27] in terms of simplicity of implementation and convergence. Secondly, the model reported here incorporates the estimation of the thermodynamic metal ion/resin partition coefficients through the Gibbs-Donnan model [29, 37], as well as the interpretation of the overall internal diffusion coefficients in terms of fast, reversible binding of metal ions to the Chelex 100 functional groups within the resin phase. Finally, the model is used to describe experimental data of Cd(II) sorption on Chelex 100 and proves successful at describing the effects of experimental conditions (stirring rate, pH, ionic strength, volume of sorbent, etc.) with a minimum number of fitted empirical variables (basically, the thickness of the diffusion boundary layer).

2. The Mixed Control Model (MCM)

2.1 Derivation of the Mixed Control Model

Let us consider the sorbent material as constituted by an ensemble of perfectly spherical beads, homogeneous in size and composition, with radius r_0.

At time t=0, the beads (initially without any metal) are plunged into a uniformly stirred metal ion solution at a given concentration $c_{\mathrm{M}}^{*}(t=0)$, where the superscript * represents the local value of the concentration at a sufficiently large distance from the beads, *i.e.:* $c_{\mathrm{M}}^{*}(t)=c_{\mathrm{M}}(t, r>r_1)$ (see Fig. 1). In solution, the metal is present exclusively as free hydrated metal cations.

As time proceeds, the metal ions in solution diffuse into the beads and therefore $c_{\mathrm{M}}^{*}(t)$ diminishes, since the solution volume is finite. The rate of metal depletion in bulk solution derives from the following treatment in the solution and particle domains.

FILM DOMAIN

Due to the stirring under laminar regime, bulk concentrations are restored at a distance r_1 from the centre of the bead, defining a film domain. Migration applies whenever there is a drop of the electrostatic potential created by the charges of the resin bead. The "effective" distance of the potential drop from the resin solution interface is of the order of the Debye length [38] which is less than 10 nm for the smallest ionic strength considered in this work. The thickness of the film domain depends on the stirring, but is assumed to be of the order of 10^{-6}m. Thus, migration is implicitly included via the Donnan partitioning (see eqn. (18) below), a reasonable approximation when the concentration of the metal cation is negligible with respect to the salt background. We also assume that diffusion in the boundary solution film in contact with the beads reaches instantaneously a quasi-steady state [2, 39] (*i.e.*, diffusion across the film is much faster than the concentration changes in bulk solution due to depletion).

$$J = D_{\mathrm{M}} \frac{c_{\mathrm{M}}^{*}(t) - c_{\mathrm{M}}\left(r_0^{+}, t\right)}{\delta} \tag{1}$$

where r_0^{+} denotes the position at the solution side of the bead/solution interface, D_{M} is the diffusion coefficient of the free metal in solution, and δ is the effective thickness of the Diffusive Boundary Layer (DBL), (see Fig. 1; the definition of each parameter is listed in the Nomenclature section). If bulk concentrations are assumed to be restored at a distance r_1 from the centre of the bead

$$\delta = \frac{r_0}{r_1}\left(r_1 - r_0\right) \tag{2}$$

PARTICLE DOMAIN

As in the film domain, the Donnan model assumes that the electrostatic potential is constant inside the bead and the transport is only due to diffusion. We also assume that diffusion of the trace ion is not distorted by the exchangeable counterions, because Na^+ ions present in the resin and solution phases are in great excess with respect to the trace metal.

The addition of the continuity equations for free and resin-bound metal cancels out the kinetic terms and yields

$$\frac{\partial \tilde{c}_{\mathrm{M,free}}\left(r,t\right)}{\partial t} + \frac{\partial \tilde{c}_{\mathrm{MR}}\left(r,t\right)}{\partial t} = \tilde{D}_{\mathrm{M}} \nabla^2 \tilde{c}_{\mathrm{M,free}}\left(r,t\right) + \tilde{D}_{\mathrm{MR}} \nabla^2 \tilde{c}_{\mathrm{MR}}\left(r,t\right) \qquad r < r_0 \tag{3}$$

(the tilde denotes parameters corresponding to the resin phase).

If we assume equilibrium in the formation of labile 1:1 complexes ($\widetilde{\mathrm{MR}}$) between metal ions and resin groups:

$$\widetilde{\mathrm{M}} + \widetilde{\mathrm{R}} \rightleftharpoons \widetilde{\mathrm{MR}}$$

(*i.e.*: the exchange reaction between the metal ions and the counterions of the resin's functional groups is very fast), then

$$\tilde{c}_{\mathrm{MR}}\left(r,t\right) = \tilde{K}_{\mathrm{MR}}\ \tilde{c}_{\mathrm{R}}\left(r,t\right) \tilde{c}_{\mathrm{M,free}}\left(r,t\right) \tag{4}$$

where $\tilde{K}_{\mathrm{MR}}$ is the conditional stability constant of the complex between the metal ion and the active groups of the resin, and $\tilde{c}_{\mathrm{R}}$ is the instantaneous local concentration of resin active sites.

Let $\tilde{c}_{\mathrm{T,M}}\left(r,t\right) = \tilde{c}_{\mathrm{M,free}}\left(r,t\right) + \tilde{c}_{\mathrm{MR}}\left(r,t\right)$ denote the local total metal concentration inside the resin at time *t* and distance *r* from the centre of the bead.

Assuming excess of resin sites (*i.e.*, $\tilde{c}_{\mathrm{R}}(r,t) \approx \text{constant}$), and taking into account that the bound metal ion is immobile (i.e. $\tilde{D}_{\mathrm{MR}} = 0$), eqn. (3) becomes

$$\frac{\partial \tilde{c}_{\mathrm{T,M}}(r,t)}{\partial t} = \nabla^2\left(\tilde{D}_{\mathrm{M}}\tilde{c}_{\mathrm{M,free}}(r,t) + \tilde{D}_{\mathrm{MR}}\tilde{c}_{\mathrm{MR}}(r,t)\right) = \tilde{D}_{\mathrm{M}}\left(\frac{1}{1+\tilde{K}_{\mathrm{MR}}\tilde{c}_{\mathrm{R}}}\right)\nabla^2\tilde{c}_{\mathrm{T,M}}(r,t) = \tilde{D}\,\nabla^2\tilde{c}_{\mathrm{T,M}}(r,t) \tag{5}$$

where

$$\tilde{D} = \frac{\tilde{D}_{\mathrm{M}}}{1+\tilde{K}_{\mathrm{MR}}\tilde{c}_{\mathrm{R}}} \tag{6}$$

is the overall (total metal) diffusion coefficient inside the resin, i.e. the "effective" diffusion coefficient for the ensemble of metal species inside the bead.

Eqn. (5) indicates that the diffusion and reaction of the free metal ions inside the bead can be re-formulated as a diffusion problem where the total metal species $\tilde{c}_{\mathrm{T,M}}(r,t)$ has an effective diffusion coefficient given by Eqn. (6), which is lower than that of the free ions. This approximation is valid whenever the reaction is fast enough to assume local instantaneous equilibrium and there is excess of resin sites.

The initial condition for eqn. (5) is:

$$\tilde{c}_{\mathrm{T,M}}(r, t=0) = 0 \qquad \forall r \le r_0 \tag{7}$$

and one boundary condition is null flux at the centre of the bead

$$\left(\frac{\partial \tilde{c}_{\mathrm{T,M}}}{\partial r}\right)_{r=0} = 0 \qquad r = 0 \quad \forall t \tag{8}$$

Due to the coupling with the solution domain, the second boundary condition (at $r = r_0$), splits into two parts, the first associated with the concentration and another with the flux.

The concentration relationship corresponds to an instantaneous equilibrium at the solid-liquid interface, determined by the partition coefficient κ [30] which accounts for the

electrostatic partitioning associated to the potential drop at $r = r_o$ and the chemical binding to the resin sites in equilibrium conditions (see Section "Theoretical interpretation of $\widetilde{D}$")

$$\tilde{c}_{\mathrm{T,M}}\left(r_0^-,t\right)=\kappa\, c_{\mathrm{M}}\left(r_0^+,t\right) \tag{9}$$

where $\tilde{c}_{\mathrm{T,M}}\left(r_0^-,t\right)$ and $c_{\mathrm{M}}\left(r_0^+,t\right)$ are the (total and free) metal concentrations at the interface in the resin and aqueous phases, respectively. The value of κ depends on pH and ionic strength, but not on the local metal concentration, as it is assumed that the amount of resin functional groups is in excess with respect to the total moles of metal (linear isotherm).

The flux condition prescribes continuity of fluxes at the interface:

$$J=\tilde{D}\left(\frac{\partial\tilde{c}_{\mathrm{T,M}}}{\partial r}\right)_{r=r_0^-}=D_{\mathrm{M}}\left(\frac{\partial c_{\mathrm{M}}}{\partial r}\right)_{r=r_0^+}=D_{\mathrm{M}}\frac{c_{\mathrm{M}}^{*}(t)-c_{\mathrm{M}}\left(r_0^+,t\right)}{\delta} \tag{10}$$

- Finally, the finite volume conditions are ensured through the mass balance constrain (where V_T and V_R are, respectively, the total volume and the volume of the resin phase):

$$\left(V_{\mathrm{T}}-V_{\mathrm{R}}\right)c_{\mathrm{M}}^{*}(0)=\frac{3V_{\mathrm{R}}}{r_0^3}\int_0^{r_0}\tilde{c}_{\mathrm{T,M}}(r,t)\,r^2dr+c_{\mathrm{M}}^{*}(t)\left(V_{\mathrm{T}}-V_{\mathrm{R}}\right) \tag{11}$$

which approximates the concentration of metal in the DBL as the bulk value (a discussion on the accuracy of this assumption is included in the Supplementary Information (SI), see Section: "Contribution of the metal in the DBL to the mass balance according to two variants of the MCM ").

MATHEMATICAL SOLUTIONS

The continuity equation (5), with initial condition (7) and boundary conditions associated to (8), (9) and (10), and restriction (11) can be solved via numerical inversion of the expression for the concentration in the Laplace space.

To obtain a simple analytical expression one can take the approximation:

$$\coth\left(\sqrt{\frac{s}{\tilde{D}}}r_0\right) \approx 1 \tag{12}$$

(*s* being the variable in the Laplace transform) which is clearly valid for $\tilde{D} \ll \frac{r_0^2}{t}$. Note that, in the least favourable conditions, we estimate a value of $\frac{r_0^2}{\tilde{D}} = 19$ h, which is much greater than the largest time recorded during the kinetic experiments. Eqn. (12) is parallel to other approaches where semi-infinite diffusion in the spherical domain is assumed [40-42].

In this way, the following equation can be derived (see details in the Section "Mathematical formulation of the mixed control model " of the SI):

$$\begin{aligned} c_{\mathrm{M}}^{*}(t) = \frac{c_{\mathrm{M}}^{*}(0)}{3Bi_{\mathrm{m}}w}\Bigg[& \frac{(Bi_{\mathrm{m}}-1)R_1+1}{R_1(R_1-R_2)(R_1-R_3)}F\left(-\frac{\sqrt{\tilde{D}t}}{r_0R_1}\right) + \\ & + \frac{(Bi_{\mathrm{m}}-1)R_2+1}{R_2(R_1-R_2)(R_3-R_2)}F\left(-\frac{\sqrt{\tilde{D}t}}{r_0R_2}\right) \\ & + \frac{(Bi_{\mathrm{m}}-1)R_3+1}{R_3(R_1-R_3)(R_2-R_3)}F\left(-\frac{\sqrt{\tilde{D}t}}{r_0R_3}\right)\Bigg] \end{aligned} \tag{13}$$

where the factors R_1, R_2 and R_3 are the roots of:

$$x^3 - x^2 + \frac{1-Bi_{\mathrm{m}}}{3Bi_{\mathrm{m}}w}x - \frac{1}{3Bi_{\mathrm{m}}w} = 0 \tag{14}$$

,

the mass transfer Biot number is defined as

$$Bi_{\mathrm{m}} = \frac{D_{\mathrm{M}}r_0}{\delta\tilde{D}\kappa} \tag{15}$$

and

$$F(x) = \mathrm{e}^{x^2}\,\mathrm{Erfc}(x) \tag{16}$$

Throughout this article, the sorption data are expressed in terms of the fractional attainment of equilibrium *f*, which is defined as the ratio between the instantaneous and final (at equilibrium) amounts of metal sorbed in the resin [30]. It can be directly computed from the experimental data as:

$$f = \frac{\left\langle \tilde{c}_{\mathrm{M}}(t) \right\rangle}{\tilde{c}_{\mathrm{M}}(\infty)} = \frac{c^*_{\mathrm{M}}(0) - c^*_{\mathrm{M}}(t)}{c^*_{\mathrm{M}}(0) - c^*_{\mathrm{M}}(\infty)} \quad ; \quad 0 \le f \le 1 \tag{17}$$

Where $\left\langle \tilde{c}_{\mathrm{M}}(t) \right\rangle$ represents the average metal concentration in the resin. This parameter *f* has the advantage that normalizes the kinetic data with respect to the initial and equilibrium bulk concentrations, which is useful for comparison among experiments. The main drawback of this notation is that it does not show properly the details of the experimental curves at relatively long times (close to equilibrium), which may be inconvenient for fitting purposes. For this reason, the results will be represented as $\ln(1-f)$ *vs*. time, where the starting point of the experiments is $\ln(1-f)=0$ and equilibrium is asymptotically reached at $\ln(1-f) \to -\infty$. An additional advantage of this representation is that, according to the FDM model, $\ln(1-f)$ depends linearly on time (eq. SI.49), thus discriminating between MCM and FDM.

Fig. *2* compares several solutions of the MCM for a typical set of parameters. Note that the numerical inversion of the Laplace solution agrees with the exact analytical solution given in [27], eq. (SI.22), as expected. One of the drawbacks of this exact analytical solution is the long computation times required for some sets of parameters. For instance, with a standard personal computer, it took 7 minutes to calculate the 300 points used to draw the curve in Fig. 2, with κ=3.63×10^3, while several hours were

needed for κ=10^8. On the other hand, the new approximate solution (13) required less than 1 minute to complete the same calculations. Moreover, the accuracy of this approximate expression is excellent at relatively short times, while the deviations from the exact solution are only relevant when approaching equilibrium (*i.e.*: f > 0.99), but still below the order of magnitude of the experimental uncertainty, and without practical consequences in the testing conditions of this work.

2.2 Theoretical interpretation of $\widetilde{D}$

As the polymer in the beads bears negative charge, a Donnan potential will develop at the bead/solution interface. The Donnan partitioning factor, χ, can be expressed as:

$$\chi^2 = \frac{\tilde{c}_{\mathrm{M,free}}\left(r_0^-,t\right)}{c_{\mathrm{M}}\left(r_0^+,t\right)} = \frac{\tilde{c}_{\mathrm{T,M}}\left(r_0^-,t\right)\Big/\left(1+\tilde{K}_{\mathrm{MR}}\tilde{c}_{\mathrm{R}}\right)}{c_{\mathrm{M}}\left(r_0^+,t\right)} \tag{18}$$

where the exponent takes into account the divalent nature of Cd^{2+} ions.

In this way, the global partitioning factor κ can be interpreted as the product of an electrostatic and a chemical binding term [43]:

$$\kappa = \chi^2\left(1+\tilde{K}_{\mathrm{MR}}\tilde{c}_{\mathrm{R}}\right) \tag{19}$$

Thus, eqn. (6) becomes

$$\tilde{D} = \frac{\chi^2\,\tilde{D}_{\mathrm{M}}}{\kappa} \tag{20}$$

The polymeric matrix is expected to reduce the mobility of the metal ion ($\tilde{D}_{\mathrm{M}}$) in the bead with respect to the value in solution. In this work, a value of $\tilde{D}_{\mathrm{M}}/D_{\mathrm{M}} = 1/14$ was assumed, in agreement with the ratios reported by Fernández *et al.* [44] for divalent cations such as Cu^{2+} and Co^{2+} in a similar iminodiacetic resin (see Table SI.6) or by Dykstra et al. [45] for a variety of species. The calculation of κ and χ from the thermodynamic Gibbs-Donnan model is detailed in the section: “Selection of model parameters” below. The validity of eq. (20) was tested by comparing its results with freely fitted $\widetilde{D}$ values, as shown in Supp. Info. Section 10.

2.3 Influence of the parameters on model predictions

A series of theoretical calculations are first presented to describe the effects of the parameters V_R, r_0, κ, and $\tilde{D}$ on the modelled kinetic data. The corresponding plots of ln(1-*f*) *vs*. time (Figs. SI.1, SI.2 and SI.3) were calculated by varying each of these parameters systematically around the values used to model the experimental data.

A first inspection reveals that the plots differ from each other essentially in two aspects, the initial slope and the degree of nonlinearity (concavity). During the initial stages of the experiments, the rate of metal sorption is mostly controlled by external film diffusion. Since FDM predicts a linear behaviour of ln(1-*f*) over the entire time domain (see (SI.50)), the presence of nonlinearity in the MCM is a result of the increasing limitation of the overall sorption rate due to intraparticle diffusion. The comparison of the theoretical fluxes of metal ion across the bead/solution boundary, calculated according to FDM, IDM and MCM, allows the approximate assessment of the point of maximum concavity. Indeed, at this point, the main controlling mechanism of the sorption rate switches from film diffusion to intraparticle diffusion. The position of this crossover point is estimated as the intersection of the fluxes predicted by FDM and IDM (see Fig. 3).

Let us now review the influence of the different model parameters.

The effect of the volume of resin, V_R, is shown in Fig. SI.1a. As observed, the increase in V_R leads to a faster sorption rate, which is a straightforward result of the mass balance. In fact, an increasing volume of resin, at a constant bead radius, implies an increment in the number of particles, which means that each bead is depleting a proportionally smaller “cell” of bulk solution (while the metal ion flux and the interfacial area per bead remain constant) and, therefore, a given fractional uptake (*f*) is reached in a shorter time.

The opposite behaviour is predicted when the bead radius is varied at constant V_R: larger values of r_0 and constant total volume imply a smaller number of beads, a larger volume to be depleted by each bead and, consequently, longer equilibration times (Fig. SI.1b). In this case, the onset of the control by internal diffusion is also shifted to shorter times as the size increases, due to the growing thickness of the intraparticle domain.

In the previous two cases both FDM and MCM predict the same trend of the initial slope with the parameters being varied (V_R or r_0).

The case of κ (Fig. SI.2), however, is more involved. In order to analyse the effect of this parameter alone (*i.e.*, at constant values of $\tilde{D}$), let us consider first the two limiting cases (represented by FDM and IDM). If transport is exclusively controlled by diffusion through the external film, the time needed to reach a given value of f increases with the value of κ since the amount of metal required for equilibrium is also progressively larger. In FDM the slope of ln(1-f) *vs.* t tends asymptotically to a constant value (see the collapsing curves of log κ = 5 and log κ = 6 in Fig. SI.2a), which depends only on the V_R / V_T ratio (see eqn. (SI.46)) and not on κ.

On the other hand, in the limiting case where transport is exclusively controlled by internal diffusion, the metal ion concentration in aqueous solution at the interface is equal to the bulk value at all times (see inset of Fig *1*), and the sorption flux is determined by the gradient of the internal concentration profile at $r = r_0$ and the intraparticle diffusion coefficient. As κ increases, the local gradient of concentration at the interface becomes progressively steeper and, consequently, the flux of metal ion is enhanced (recall that these simulations are performed at constant $\tilde{D}$), which leads to an increasingly faster sorption kinetics. It is, thus, evident that FMD and IDM predict opposite trends of the kinetic profiles with κ.

In the mixed control situation, the net flux will be controlled by the slowest mechanism. Indeed, as observed in Fig. SI.2c, MCM predicts kinetic profiles that range between a predominantly FDM behaviour at large κ values, especially at short times (where ln(1-*f*) *vs. t* is almost linear) and a mostly intraparticle diffusion-limited kinetics at low κ values (where the partition coefficient is not high enough to induce a relevant decline of the metal ion concentration at the interface). As a consequence, MCM foresees an inverse trend with κ of the ln(1-*f*) slope, to the one found with FDM.

The relative predominance of the external film and internal particle diffusion controls is obviously affected also by the value of the internal diffusion coefficient, as seen in Fig. SI.3, which represents the effect on the kinetic profiles of varying values of $\tilde{D}$ at constant κ. In this case, the effect is straightforward: at small values of the internal diffusion coefficient the simulated curves approach the IDM results, whereas at large values of $\tilde{D}$ the intraparticle diffusion becomes faster (not limiting) and the behaviour tends to be better described by FDM.

Finally, one can assess the impact of the inverse relationship between κ and $\tilde{D}$ (eq. (20)) due to cation complexation inside the resin. According to this relationship, the increase in κ has opposite effects on the relative contribution of the intraparticle diffusion mechanism to the mass transport: it leads to a simultaneous increase in the concentration gradient at the interface and a decrease in the internal diffusion coefficient.

3. Materials and Methods

3.1 Experimental

Chelex 100 resin (100-200 mesh) was purchased from BioRad Laboratories. Prior to the experiments, the resin was soaked in methanol solution to remove any possible free

iminodiacetic moieties, then carefully rinsed with Milli-Q water, filtered and stored in a closed pot. All solutions were prepared in Milli-Q water.

Either a Metrohm or a Crison Cd-ISE was used to monitor the concentration of Cd^{2+} in solution during the sorption experiments. The reproducibility and reliability of these measurements were also checked by comparison with ICP-MS analysis (see SI). The Cd-ISEs were calibrated with standard Cd(II) solutions at the same ionic media used in the kinetic experiments. At least two calibration curves were performed, before and after each sorption experiment.

For each experimental condition tested, an accurately weighted amount of resin, previously dried in oven at 60º C, was equilibrated in a $NaNO_3$ solution at the desired pH and ionic strength. For experiments at circumneutral pH, the solutions were buffered with 1 mM 3-(N-morpholino)propanesulfonic acid (MOPS) (which has been reported not to complex Cd [46]) and the pertinent small additions of NaOH or HNO_3.

The sorption batch experiments were performed at 25 ± 0.1 ºC in thermostated polypropylene vessels (the resin beads adhere to glass surfaces). Since the prolonged usage of a magnetic stirrer may deteriorate the beads, the suspension was stirred from above using an OrionStar Series Automatic Stirrer Probe.

After the initial contact of the equilibrated resin with the standard Cd(II) solution, the values of Cd^{2+} concentration were recorded in continuous mode by measuring the Cd-ISE potentials at each time with a computer program specifically written in MATLAB [47].

Each experiment was performed in duplicate, and the error bars in the ln(1-*f*) data were computed from the standard deviation of the measured concentrations.

3.2 Selection of model parameters

Most parameters required by the MCM are experimentally accessible (D_M, V_R and r_0), while others were estimated indirectly from theoretical models ($\widetilde{D}$ and κ) or directly fitted from the kinetic sorption data (δ).

The value of the diffusion coefficient of Cd^{2+} ion in water, D_M, was taken from the literature [48], as 7×10^{-10} m^2/s (25º C). The values of V_R and r_0 must take into account the variation of the bead size due to the swelling/shrinking of Chelex 100 [49], which is highly sensitive to pH and ionic strength of the surrounding solution. Therefore, they were directly determined at the same experimental conditions of the sorption data, through dedicated experiments. V_R is assumed equal to the water content in the resin beads and it was determined by measuring the loss of mass of an aliquot of resin previously equilibrated in aqueous solutions at the corresponding pH and ionic strength and, then, oven-dried at 60°C until constant weight (considering the water density equal to 1 g/mL).

The radius of the resin beads, $r_{0,}$ was interpolated for each experimental condition (pH, *I*) from values determined by optical microscopy, as detailed in the SI.

The ratio κ between the concentrations of metal sorbed in the resin and that in bulk solution at equilibrium can, in principle, be calculated from experimental equilibrium data, using the following expression, derived from eq. (9) and the mass balance:

$$\kappa = \frac{(V_T - V_R)(c_M^*(0) - c_M^*(\infty))}{V_R c_M^*(\infty)} \tag{21}$$

However, the use of this equation is not convenient at acid pH values, where the amount of sorbed metal ion is negligible, or at high pH values (>6), and relatively large V_R/V_T ratios, where the values of $c_M^*(\infty)$ are affected by a large uncertainty due to analytical detection limits and/or excessively long equilibration times. Therefore, the values of κ were computed from the Gibbs-Donnan equilibrium model [29]. According to this

model, the sorbent is represented as a concentrated solution phase, separated from the external solution by an interface through which water, neutral molecules and ions can diffuse, but the active groups, permanently linked to the solid matrix, cannot. The partition coefficient of the metal ions between the two phases (K^*, in the Gibbs-Donnan nomenclature, which corresponds to κ in the present notation), is computed from the intrinsic protonation and complexation constants of the metal ion with the active groups of the resin, the pH and ionic strength (I) of the solution and the concentration of the counterion in both phases, as reported in the literature [10, 28, 29, 37, 50] (see details in the Supp. Info.. "Estimation of κ from the Gibbs-Donnan model"). Once κ is computed, the values of $c_M^*(\infty)$ required for the calculation of f in eq. (17) are obtained from eq. (21).

The effective thickness of the DBL [51, 52], δ, was considered as a fitted parameter, with the only constraint of being lower than the radius of the bead, and it was assumed to be dependent on the stirring rate only.

χ was estimated from the Donnan model using the values of the ionic strength (I) and the concentration of charged sites in the resin (q), as:

$$\chi = \frac{q}{2I} + \sqrt{\left(\frac{q}{2I}\right)^2 + 1} \qquad (22)$$

The values of q at each value of pH and I were computed as the amount of free sites (not bound to protons or Cd(II) ions) per volume of resin, according to the Gibbs-Donnan model. The total number of sites was taken equal to 1.90 mmol/g, as determined by acid-base titrations of the resin [53]. The theoretical values of χ obtained in this way were in excellent agreement with resin/solution equilibrium ratios of Rb^+ ion concentration determined experimentally (data not shown).

4. Results and discussion

This section analyzes the ability of the MCM to describe the effect of the different variables (metal ion concentration, amount of resin, size of beads, stirring rate, pH and ionic strength) on the sorption kinetics by comparison with experimental data.

4.1 Influence of $c_{\mathrm{M}}^{*}(0)$, and V_{R}.

The present derivation of the MCM assumes that the total functional groups of the resin are in excess with respect to the amount of metal ion bound at equilibrium. This condition is necessary to ensure that κ (and, consequently, $\widetilde{D}$) is invariant with respect to $\tilde{c}_{\mathrm{T,M}}(r,t)$). Under these conditions, the bulk metal ion concentration at each time, $c_{\mathrm{M}}^{*}(t)$, is strictly proportional to the initial concentration, $c_{\mathrm{M}}^{*}(0)$, which leads to the fractional attainment of equilibrium f being independent of the initial metal ion concentration (SI.36**)**. This expectation was confirmed from experiments at different initial Cd(II) concentrations (while keeping constant all other conditions) in the range 1×10^{-6} M to 1×10^{-4} M. In these conditions, the kinetic profiles collapsed on the same master curve, which demonstrates that the sorption data can be effectively normalised using the descriptor *f*. For instance, Fig. 4a shows how the effect of a 2.5-fold increase in $c_{\mathrm{M}}^{*}(0)$ leads to negligible differences in *f* within the experimental uncertainty. As a reference, at $c_{\mathrm{M}}^{*}(0)$ $=5\times10^{-5}$ M and with the amount of resin used in the experiments, the ratio bound metal ion/Chelex 100 groups at equilibrium is estimated as 0.05. The experimental data also show a good reproducibility in the whole range selected for model fitting throughout this work. Uncertainty increases significantly as *f* gets closer to 1, due to accumulated experimental errors and the constraint of the analytical limit of detection.

Let us now comment on the ability of the MCM to account for the influence of the amount of resin on the experimental kinetic profiles. As discussed in the section

"Influence of the parameters on model predictions", the effect of V_R is a direct consequence of the mass balance constrain. Fig 4b shows a representative example of the influence of a 5-fold increase in the amount of resin, compared with MCM predictions involving V_R as the only variable parameter. As expected, the increase in the volume of resin leads to an increase in the initial slope of the ln(1-*f*) plot (in absolute value), reflecting a faster kinetics. The crossover point between the predominant mechanisms of external and internal diffusion control is reached at higher *f* values, but shorter times in the experiment with the larger V_R, which is reflected by the greater curvature of the plot. In both cases, there is a good agreement between data and MCM predictions within the experimental uncertainty.

4.2 Impact of the stirring rate

To evaluate the influence of the hydrodynamic conditions on the sorption kinetics, a series of five experiments were performed at exactly the same experimental conditions except for the rate of the stirrer probe. A relatively high pH value (7.3) was chosen for this set of experiments to ensure conditions close to the regime of external diffusion control (see section "Impact of pH and ionic strength (I)" for details of the consequences of pH changes).

As shown in Fig. *5*, the sorption rate increases with the stirring speed, which indicates that the overall mass transport process is, at least partially, controlled by diffusion across the external film. This effect is accurately described by the MCM (see continuous lines in Fig. 5) as a monotonic decrease of the DBL thickness, δ, from 43.5 to 7 μm (values listed in Table 2). Note that δ is the only fitted parameter in this series of kinetic profiles.

The increasing trend of the slope of ln(1-*f*) *vs*. *t* (in absolute value) with the stirring rate is due to the increased concentration gradient across the DBL (and, consequently, a

larger metal flux) associated with the decline in δ, which is obviously consistent also with the predictions of FDM. However, some deviation from linearity is observed at the highest stirring speeds, where the relative contribution of the internal mass transfer resistance is largest; this behaviour can only be described by the MCM.

4.3 Impact of pH and ionic strength (I)

The influences of pH and ionic strength on the metal ion sorption kinetics are related to each other, as both variables regulate the degree of protonation of the resin which, in turn, determines: i) the variation in the physical structure of the beads due to the swelling/shrinking phenomena (reflected on the values of V_R and r_0); and ii) the effective metal binding properties of the resin (κ) and, indirectly, the internal diffusion coefficient $\widetilde{D}$ (see section "Influence of the parameters on model predictions").

The effect of pH was first studied through a series of experiments performed at the same ionic strength and mass of dry resin in the range $3.5 \leq$ pH ≤ 7.4, since at pH < 3.5 the fraction of metal ion sorbed on the resin is too low (less than 1% of total Cd(II)) to allow accurate measurements of the depletion rate in bulk solution. The upper limit of pH 7.4 was selected to prevent precipitation of Cd(II) hydroxydes or Cd(II) carbonates taking into account thermodynamic predictions of Visual MINTEQ [54]. This upper limit could be moved to 7.5 in the case of the experiment under N_2 atmosphere (see Fig 5). The experimental results are shown in Fig. 6, together with MCM calculations using the parameter values listed in Table 3.

As seen in this figure, the overall repeatability of the measurements was good. The predictive ability of the model is remarkable, taking into account that none of the MCM parameters was specifically fitted to these data, as discussed in the following paragraphs.

The values of V_R and r_0 were determined experimentally, in absence of Cd(II), at each pH and ionic strength (as explained in the section "Selection of model parameters"), and supposed to be constant within the timescale of the experiments (consistently with the low metal/resin group ratios experimentally tested). The values of κ and $\widetilde{D}$ were calculated at each pH as detailed in the previous sections. Finally, the diffusion layer thickness (δ = 7 μm) was taken equal to the value fitted at the corresponding stirring rate in the experiments discussed in the section "Impact of the stirring rate". No evidences of variations of δ with pH or ionic strength were found.

The physicochemical interpretation (according to MCM) of the observed influence of pH on the sorption profiles follows the general ideas presented in the section "Influence of the parameters on model predictions". The kinetic data present a monotonic behaviour with pH, where the most sensitive parameters are κ and $\widetilde{D}$. At low pH values, the sorption rates are low with a distinct nonlinear behaviour of ln(1-*f*) *vs*. *t*. In these conditions, the net flux of metal across the resin/solution interface reaches a situation of control by internal diffusion at the early stages of the kinetic process, due to the relatively small values of $\widetilde{D}$ and concentration gradient inside the beads. The resulting kinetic profile resembles the simulations plotted in Fig. SI.2b for IDM. As pH increases, the sorption rates increase and, in the limit of high pH, they approach the linear behaviour predicted by FDM at large κ (see Figs. SI.2a and SI.2c). The relative influence of external film and internal diffusion controls throughout each kinetic run can be evidenced by the position of the crossover point between the FDM and IDM theoretical fluxes pointed by red arrows in Fig. 6, which are shifted to larger values of *t* and *f* as pH increases. Notice that FDM alone is not able to predict the correct trend of the experimental slope of ln(1-*f*) with pH, which represents an important support for the application of MCM to the Cd(II)/Chelex 100 system.

To study the effects of the ionic strength, a series of experiments were performed at the same pH and mass of dry resin, but at two different concentrations of background electrolyte: 0.1 M and 0.0015 M $NaNO_3$. A pH equal to 5.5 was selected since, according to the Gibbs-Donnan model, the largest variation in the protonation degree of Chelex 100, due to the change in *I*, takes place between pH 4.5 and 6.5. The resulting experimental curves are shown in Fig. 7, while the fitting parameters are listed in Table 3 (experiments 3 and 6).

At low concentration of background electrolyte, the ln(1-*f*) function behaves almost linearly (especially at short times), with a high sorption rate. This can be explained as a consequence of the reduced electrostatic screening inside the resin. The lower ionic strength induces swelling of the beads due to increased repulsion among the negatively charged iminodiacetic groups of Chelex 100 and, consequently, slightly increased values of V_R and r_0 are obtained (Table 3). These parameters have an opposite impact on the sorption rates (see Fig. SI.1) and, consequently, their combined influence on the observed effect is secondary. On the other hand, the reduced electrolyte screening at low ionic strength leads to stronger interactions of the metal ions with the active sites of the resin and, thus, to a larger partitioning coefficient at the interface (κ), which seems to be the prevailing effect (a change in two orders of magnitude is observed, as listed in Table 3). As a consequence, the kinetic curve at low ionic strength approaches the FDM behaviour, in a similar way to the sorption rates found at higher pH. Indeed, it must be noted that the model parameters for κ and $\widetilde{D}$ at I = 0.0015 M and pH 5.52 could (from interpolation of the data listed in Table 3) correspond to those at I = 0.1 M and an approximate pH of 7.

The study of the dynamics of the local metal concentration in the system provides further insight into the controlling transport mechanisms behind the process of

accumulation. Fig. 8 shows the normalized concentration profiles in the resin phase and in the adjacent diffusive boundary layer as a function of contact time at the lowest and highest pH values. Note that, from previous discussion, the profiles at the highest pH are also representative of equivalent systems at low ionic strength and lower pH values. At pH 7.5 (lower panels in Fig. *8*) the binding affinity of the resin groups is large enough so that the local concentration in the solution region adjacent to the interface remains effectively exhausted throughout the timescale of the experiment. This means that a perfect sink behaviour holds and the sorption rate remains close to the value predicted by the film diffusion model. The concentration profiles calculated at pH 3.48 (upper panels in Fig. *8*) are characteristic of a system that exhibits a transition between external film and internal diffusion control. In very initial stages (*e.g.*, 1 s) there is an almost complete exhaustion of metal ions in the solution region adjacent to the interface ($c_{\mathrm{M}}\left(r_0^+,t\right)\approx 0$), and, thus, the resin bead acts as a perfect sink. As time proceeds, the increase of the concentration at $r=r_0^+$ leads to a flattening of the gradient in the DBL (see *e.g*. the profile at 100 s), which is also facilitated by the metal ion depletion in bulk solution. At subsequent stages, the metal ion profile along the DBL becomes almost flat (see *e.g*. the concentration profile at 1500 s) and the resistance to the mass transport in the external film becomes progressively smaller, whereas the internal concentration gradient is still significant and, therefore, the overall flux converges to the limiting value under control by internal diffusion.

5. Conclusions

An approximate analytical solution for the Mixed Control Model (MCM) (eqn. (13))is here reported to describe the rate of metal ion sorption by a chelating sorbent in finite volume conditions, where the transport is limited by both internal and external diffusion. This analytical expression is accurate up to relatively large values of

fractional attainment of equilibrium, and it can be easily computed even with a standard spreadsheet application (see file provided as Supporting Information).

The proposed MCM has a good descriptive and predictive capability, being able to account for the effects of several experimental variables such as pH and ionic strength with just one empirical parameter (the DBL thickness). A substantial improvement over the classical film diffusion model (FDM) was obtained by considering the intraparticle diffusion, which can account for the deviation from the theoretical linear behaviour at low pH values and gives some insights about the physicochemical mechanisms of sorption. The effective diffusion coefficient in the resin can be computed from thermodynamic resin/solution partition ratios calculated by the Gibbs-Donnan model (see eqns.(6) and (20)).

Although precaution is advised against the extrapolation of this model to more complex systems (*e.g*. large concentrations of electrolytes leading to resin saturation, or presence of non-labile metal-ligand complexes in solution), the observed proton competition effect might be similar to the effect of other competing background ions (such as Mg(II) or Ca(II)).

Acknowledgments

The authors gratefully acknowledge support for this research from the Spanish Ministry MINECO (Projects CTM2013-48967 and CTM2016-78798) and by the "Comissionat d'Universitats i Recerca de la Generalitat de Catalunya" (2014SGR1132). FQ acknowledges a grant from AGAUR.

6. References

[1] P.S. Walsh, D.A. Metzger, R. Higuchi, Chelex 100 as a Medium for Simple Extraction of DNA for PCR-Based Typing from Forensic Material, Biotechniques 54 (2013) 134-139.
[2] A. Zagorodni, Ion Exchange Materials: Properties and Applications, Elsevier, Oxford, 2007.
[3] Inamuddin, M. Luqman (Eds.), Ion-exchange technology. II, Applications, Springer, Dordrecht, 2012.

[4] J.L. Cortina, A. Warshawsky, N. Kahana, V. Kampel, C.H. Sampaio, R.M. Kautzmann, Kinetics of goldcyanide extraction using ion-exchange resins containing piperazine functionality, React. Funct. Polym. 54 (2003) 25-35.
[5] M. Pesavento, R. Biesuz, Simultaneous Determination of Total and Free Metal-Ion Concentration in Solution by Sorption on Iminodiacetate Resin, Anal. Chem. 67 (1995) 3558-3563.
[6] P. Pohl, Application of ion-exchange resins to the fractionation of metals in water, TrAC, Trends Anal. Chem. 25 (2006) 31-43.
[7] N. Manouchehri, S. Besançon, A. Bermond, Kinetic characterizing of soil trace metal availability using Soil/EDTA/Chelex mixture, Chemosphere 83 (2011) 997-1004.
[8] S. Leguay, P.G.C. Campbell, C. Fortin, Determination of the free-ion concentration of rare earth elements by an ion-exchange technique: implementation, evaluation and limits, Environ. Chem. 13 (2016) 478-488.
[9] Z.Q. Shi, P. Wang, L.F. Peng, Z. Lin, Z. Dang, Kinetics of Heavy Metal Dissociation from Natural Organic Matter: Roles of the Carboxylic and Phenolic Sites, Environ. Sci. Technol. 50 (2016) 10476-10484.
[10] M. Pesavento, A. Profumo, R. Biesuz, G. Alberti, Ion exchange complexing resins as sensors for the determination of free metal ion concentration at a low level, Solvent Extr. Ion Exch. 26 (2008) 301-320.
[11] R. Tantra, H. Bouwmeester, E. Bolea, C. Rey-Castro, C.A. David, J.-M. Dogné, J. Jarmann, F. Laborda, J. Laloy, K.N. Robinson, A.K. Undas, M. van der Zande, Assessing Suitability of Analytical Methods to Measure Solubility for the Purpose of Nano-Regulation, Nanotoxicology 10 (2016) 173-184.
[12] W. Davison, H. Zhang, In-Situ Speciation Measurements of Trace Components in Natural-Waters Using Thin-Film Gels, Nature 367 (1994) 546-548.
[13] S. Mongin, R. Uribe, C. Rey-Castro, J. Cecília, J. Galceran, J. Puy, Limits of the Linear Accumulation Regime of DGT Sensors, Environ. Sci. Technol. 47 (2013) 10438-10445.
[14] H. Zhang, W. Davison, Use of diffusive gradients in thin-films for studies of chemical speciation and bioavailability, Environ. Chem. 12 (2015) 85-101.
[15] J. Galceran, J. Puy, Interpretation of diffusion gradients in thin films (DGT) measurements: a systematic approach, Environ. Chem. 12 (2015) 112-122.
[16] H. Yin, M. Han, W. Tang, Phosphorus sorption and supply from eutrophic lake sediment amended with thermally-treated calcium-rich attapulgite and a safety evaluation, Chem. Eng. J. 285 (2016) 671-678.
[17] J. Puy, J. Galceran, S. Cruz-Gonzalez, C.A. David, R. Uribe, C. Lin, H. Zhang, W. Davison, Measurement of Metals Using DGT: Impact of Ionic Strength and Kinetics of Dissociation of Complexes in the Resin Domain, Anal. Chem. 86 (2014) 7740-7748.
[18] M. Jimenez-Piedrahita, A. Altier, J. Cecilia, C. Rey-Castro, J. Galceran, J. Puy, Influence of the settling of the resin beads on diffusion gradients in thin films measurements, Anal. Chim. Acta 885 (2015) 148-155.
[19] J. Puy, J. Galceran, C. Rey-Castro, Interpreting the DGT Measurement: Speciation and Dynamics, in: W. Davison (Ed.) Diffusive Gradients in Thin-Films for Environmental Measurements, Cambridge University Press, Cambridge, 2016, pp. 93-122.
[20] A. Altier, M. Jiménez-Piedrahita, C. Rey-Castro, J. Cecilia, J. Galceran, J. Puy, Accumulation of Mg to Diffusive Gradients in Thin Films (DGT) Devices: Kinetic and Thermodynamic Effects of the Ionic Strength, Anal. Chem. 88 (2016) 10245-10251.
[21] V.J. Inglezakis, S.G. Poulopoulos, Adsorption, Ion Exchange and Catalysis. Design of Operations and Environmental Applications, Elsevier, Amsterdam 2006.
[22] F.G. Helfferich, Ion exchange, Dover Publications, New York, 1995.
[23] V.J. Inglezakis, H.P. Grigoropoulou, Applicability of simplified models for the estimation of ion exchange diffusion coefficients in zeolites, J. Colloid Interface Sci. 234 (2001) 434-441.
[24] J. Crank, The mathematics of diffusion, 2nd ed., Clarendon Press, Oxford, 1975.
[25] C.E. Harland, Ion-exchange : theory and practice, 2nd ed., Royal Society of Chemistry, London, 1994.
[26] Inamuddin, M. Luqman (Eds.), Ion-exchange technology. I, Theory and Materials, Springer, Dordrecht, 2012.
[27] M.D. LeVan, G. Carta, Adsorption and Ion Exchange, in: D.W. Green, R.H. Perry (Eds.) Perry's chemical engineers' handbook, McGraw-Hill, New York, 2008, pp. 1-69.
[28] G. Alberti, R. Biesuz, EmporeTM membrane vs. Chelex 100: Thermodynamic and kinetic studies on metals sorption, React. Funct. Polym. 71 (2011) 588-598.

[29] G. Alberti, V. Amendola, M. Pesavento, R. Biesuz, Beyond the synthesis of novel solid phases: Review on modelling of sorption phenomena, Coord. Chem. Rev. 256 (2012) 28-45.
[30] G.E. Boyd, A.W. Adamson, L.S. Myers, The Exchange Adsorption of Ions from Aqueous Solutions by Organic Zeolites .2. Kinetics, J. Am. Chem. Soc. 69 (1947) 2836-2848.
[31] S. Paterson, The Heating or Cooling of a Solid Sphere in a Well-Stirred Fluid, Proc. Phys. Soc. London 59 (1947) 50-58.
[32] V.V. Krongauz, C.W. Kocher, Kinetics of ion exchange in monodisperse resin, J. Appl. Polym. Sci. 65 (1997) 1271-1283.
[33] G. Atun, G. Hisarli, A.E. Kurtoglu, N. Ayar, A comparison of basic dye adsorption onto zeolitic materials synthesized from fly ash, J. Hazard. Mater. 187 (2011) 562-573.
[34] A. Hosseini-Bandegharaei, M.S. Hosseini, M. Sarw-Ghadi, S. Zowghi, E. Hosseini, H. Hosseini-Bandegharaei, Kinetics, equilibrium and thermodynamic study of Cr(VI) sorption into toluidine blue o-impregnated XAD-7 resin beads and its application for the treatment of wastewaters containing Cr(VI), Chem. Eng. J. 160 (2010) 190-198.
[35] D. Petruzzelli, L. Liberti, R. Passino, F.G. Helfferich, Y.L. Hwang, Chloride Sulfate Exchange Kinetics - Solution for Combined Film and Particle Diffusion Control, React. Polym. 5 (1987) 219-226.
[36] J.J. Grossman, A.W. Adamson, The Diffusion Process for Organolite Exchangers, J. Phys. Chem. 56 (1952) 97-100.
[37] M. Pesavento, R. Biesuz, M. Gallorini, A. Profumo, Sorption Mechanism of Trace Amounts of Divalent Metal-Ions on a Chelating Resin Containing Iminodiacetate Groups, Anal. Chem. 65 (1993) 2522-2527.
[38] H. Ohshima, Theory of colloid and interfacial electric phenomena, 1st ed., Elsevier Academic Press, Amsterdam ; Boston, 2006.
[39] J. Galceran, J. Monne, J. Puy, H.P. van Leeuwen, Transient biouptake flux and accumulation by microorganisms: The case of two types of sites with Langmuir adsorption, Mar. Chem. 99 (2006) 162-176.
[40] T.R. Brumleve, J. Osteryoung, Spherical Diffusion and Shielding Effects in Reverse Pulse Voltammetry, J. Phys. Chem. 86 (1982) 1794-1801.
[41] S.Y. Park, K. Aoki, K. Tokuda, H. Matsuda, Determination of Diffusion-Coefficients of Metals Dissolved in Mercury by Double Potential Step Chronoamperometry at Hanging Mercury Drop Electrodes, Bull. Chem. Soc. Jpn. 56 (1983) 2133-2137.
[42] J. Galceran, J. Salvador, J. Puy, F. Mas, D. Gimenez, M. Esteban, Amalgamation effects in reverse pulse polarography at spherical electrodes. Influence on speciation measurements, J. Electroanal. Chem. 442 (1998) 151-167.
[43] N. Fatin-Rouge, A. Milon, J. Buffle, R.R. Goulet, A. Tessier, Diffusion and partitioning of solutes in agarose hydrogels: The relative influence of electrostatic and specific interactions, J. Phys. Chem. B 107 (2003) 12126-12137.
[44] A. Fernandez, M. Diaz, A. Rodrigues, Kinetic Mechanisms in Ion-Exchange Processes, Chem. Eng. J. 57 (1995) 17-25.
[45] J.E. Dykstra, P.M. Biesheuvel, H. Bruning, A. Ter Heijne, Theory of ion transport with fast acid-base equilibrations in bioelectrochemical systems, Phys Rev E 90 (2014).
[46] C.M.H. Ferreira, I.S.S. Pinto, E.V. Soares, H.M.V.M. Soares, (Un)suitability of the use of pH buffers in biological, biochemical and environmental studies and their interaction with metal ions - a review, Rsc Adv 5 (2015) 30989-31003.
[47] MATLAB Release 2012b, The MathWorks, Inc., Natick, Massachusetts, USA, 2012.
[48] CRC Handbook of Chemistry and Physics, 97th ed., CRC Press, Boca Raton, 2016.
[49] J. Krasner, J.A. Marinsky, Dissociation of Iminodiacetic Acid Groups Incorporated in a Chelating Ion-Exchange Resin, J. Phys. Chem. 67 (1963) 2559-&.
[50] M. Pesavento, R. Biesuz, G. Alberti, M. Sturini, Separation of copper(II) and aluminium(III) from fresh waters by solid phase extraction on a complexing resin column, J. Sep. Sci. 26 (2003) 381-386.
[51] J. Galceran, H.P. van Leeuwen, Dynamics of Biouptake Processes: the Role of Transport, Adsorption and Internalisation, in: H.P. van Leeuwen, W. Köster (Eds.) Physicochemical Kinetics and Transport at Biointerfaces, John Wiley & Sons, Chichester, 2004.
[52] J.P. Pinheiro, R.F. Domingos, Impact of spherical diffusion on labile trace metal speciation by electrochemical stripping techniques, J. Electroanal. Chem. 581 (2005) 167-175.
[53] M. Pesavento, R. Biesuz, J.L. Cortina, Sorption of Metal-Ions on a Weak Acid Cation-Exchange Resin Containing Carboxylic Groups, Anal. Chim. Acta 298 (1994) 225-232.
[54] J.P. Gustafsson, Visual MINTEQ v. 3.1, 2013.

7. Figures

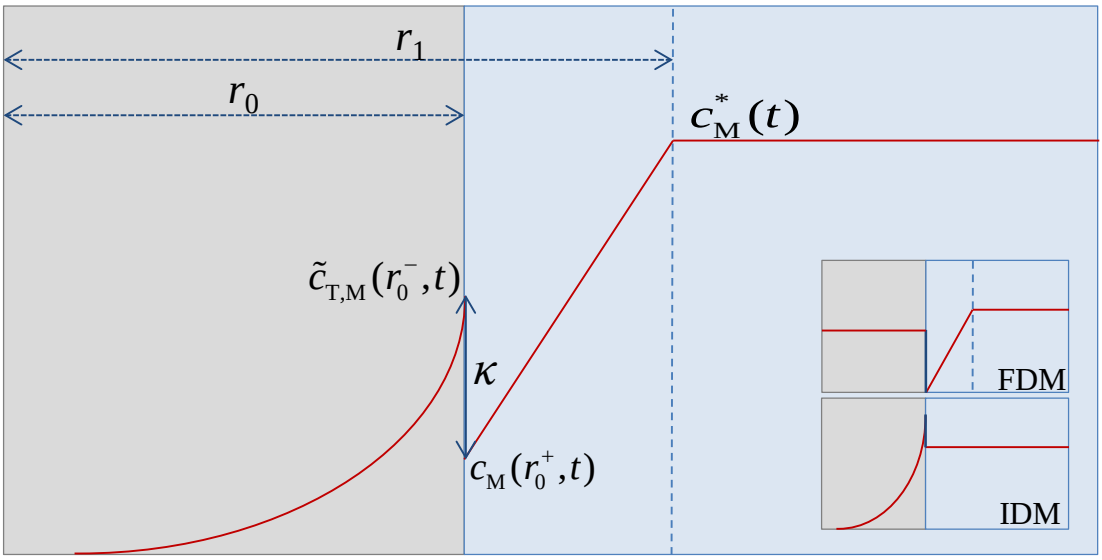

Figure 1. Schematic representation of the radial concentration profiles in the resin (grey background) and aqueous solution (blue background) phases, as expected in the MCM. The metal distributes between the two sides of the interface according to the coefficient κ*, which depends only on pH and ionic strength. The diffusive boundary layer (DBL) extends from* r_0 *to* r_1 *. The insets represent the concentration profiles as described by FDM and IDM (figures not in scale).*

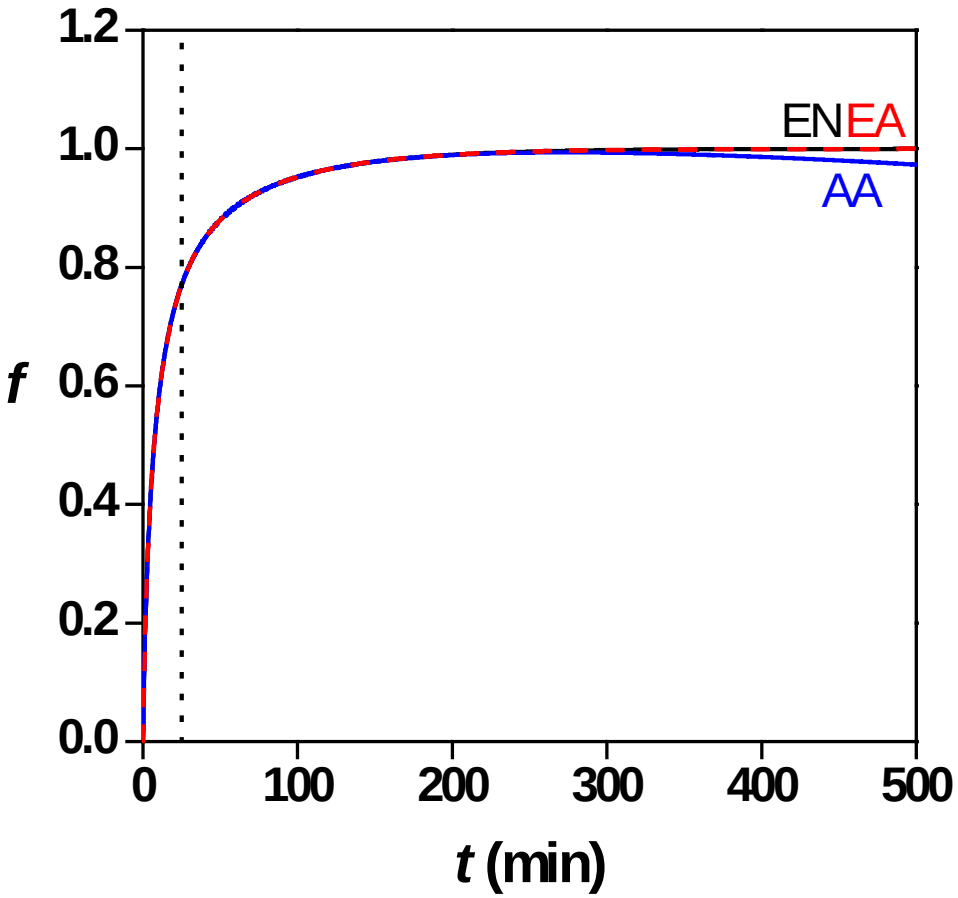

Figure 2. Comparison of the fractional approach to equilibrium f, eqn. (17) according to the Approximate Analytical solution (AA,eq. (13)), the Exact Numerical solution (EN, numerical inversion of eq. (SI.21)) and the Exact Analytical solution (EA,eq. (SI.22)) of MCM. The parameters used for the computation are listed in Table 3, experiment 1 (pH 3.48). The vertical dashed line at t= 25 min corresponds to the typical timescale considered in the experiments.

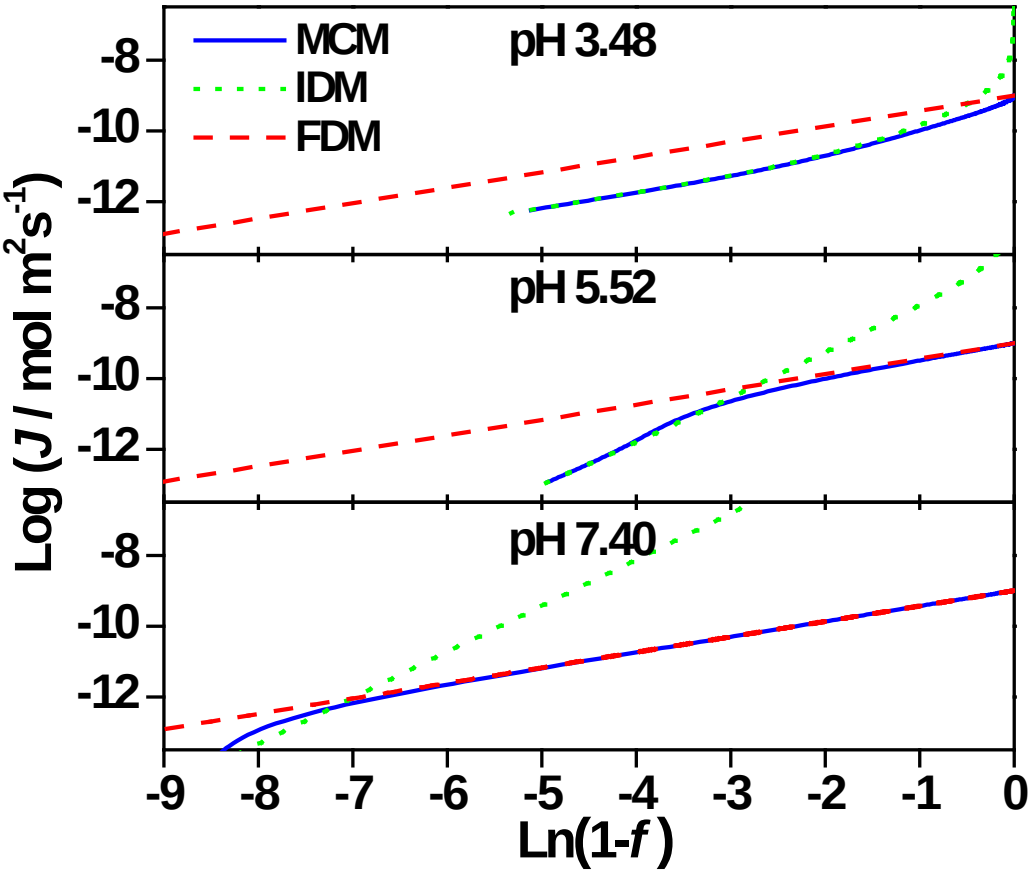

Figure 3. Fluxes J (in mol m^{-2} s^{-1}) at the particle/solution interface, expressed as a function of f, computed according to MCM (blue continuous line), IDM (green dotted line) and FDM (red dashed line) at pH 3.48, 5.52 and 7.40. The parameters used for the computations are listed in Table 3.

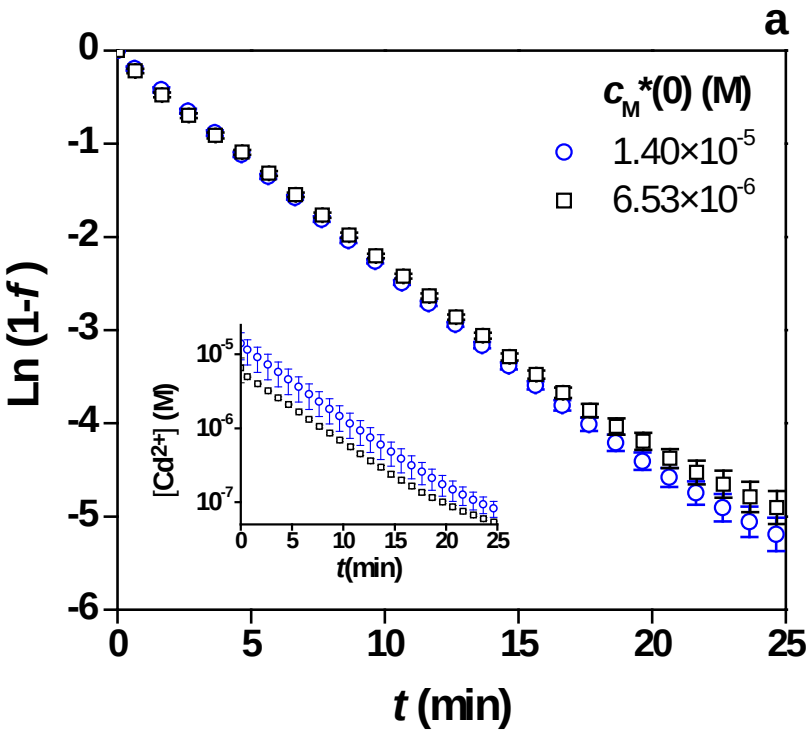
a
c_M*(0) (M)
1.40×10^{-5}
6.53×10^{-6}
Ln (1-*f*)
t (min)
[Cd^{2+}] (M)
t(min)

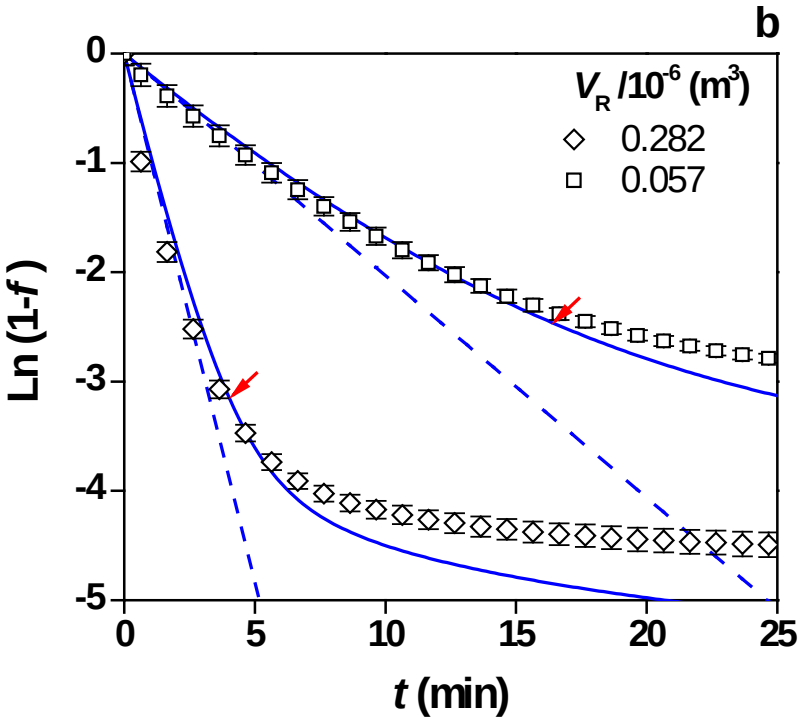
b
V_R /10^{-6} (m^3)
0.282
0.057
Ln (1-*f*)
t (min)

Figure 4. Effects of the initial metal concentration (a) and resin volume (b) on the sorption curves of Cd on Chelex-100 in 0.1M $NaNO_3$. Symbols: experimental data (average of two replicates); solid lines: MCM fits; dashed lines: FDM fits with the same parameters. (a): $c_M^*(0)$ = 1.40×10^{-5} M (blue circles) and 6.53×10^{-6} M (black squares); $m_{dry\ resin}$ = 24.5 mg; pH =7.4; the inset shows the experimental raw data (error bars correspond to standard deviation of the replicates). (b): pH: 4.55; $c_M^*(0)$ = 5×10^{-5} M; $m_{dry\ resin}$ = 24.5 mg (squares) and 121.2 mg (diamonds). The internal legend reports the values of V_R×10^6 (in m^3)

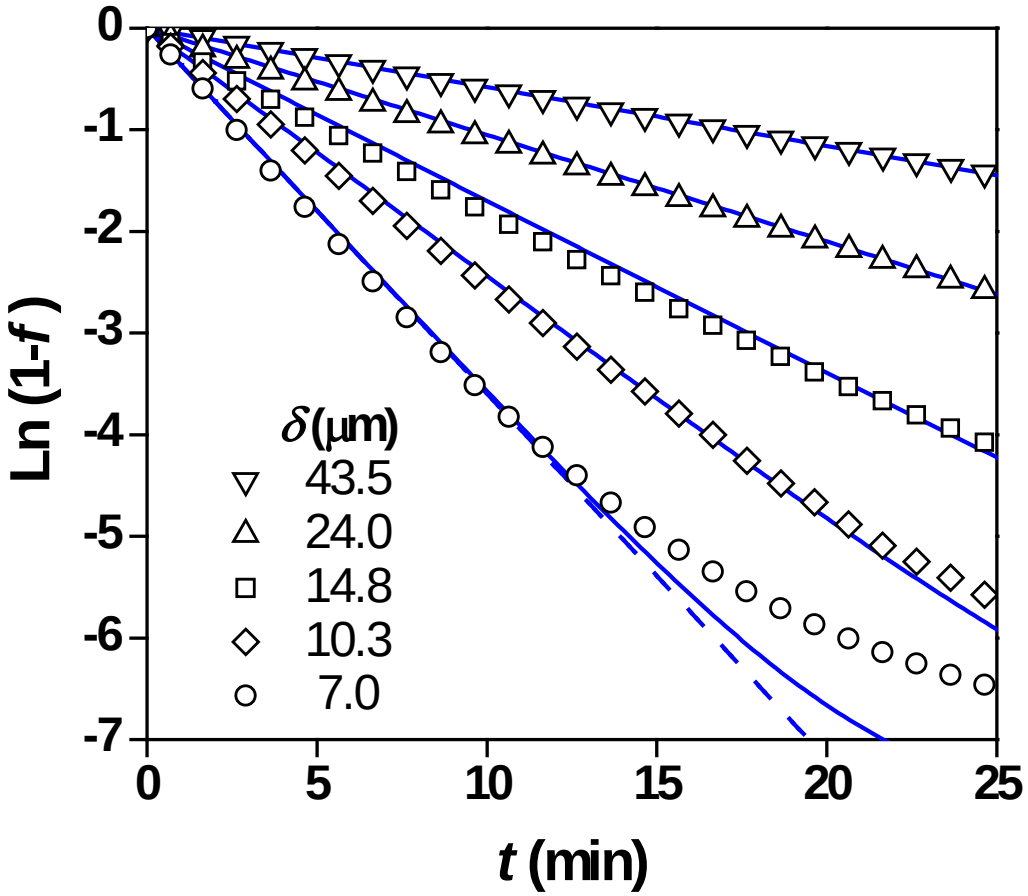

Figure 5. Sorption curves of Cd on Chelex 100 at different stirring rates. Symbols: experimental data. Solid lines: MCM fittings. In the legend the fitted values of δ, expressed in μm, are reported, each of them corresponding to one of the available settings of the stirrer. For the sake of comparison, the curve corresponding to the highest stirring rate was also calculated with FDM, using the same parameters (dashed line). Experimental conditions: pH = 7.3, Ionic Strength = 0.1M in $NaNO_3$, $m_{\text{dry resin}}$ = 36 mg, $c_M^*(0) = 5\times10^{-5}$ M. Experiments performed under N_2 atmosphere.

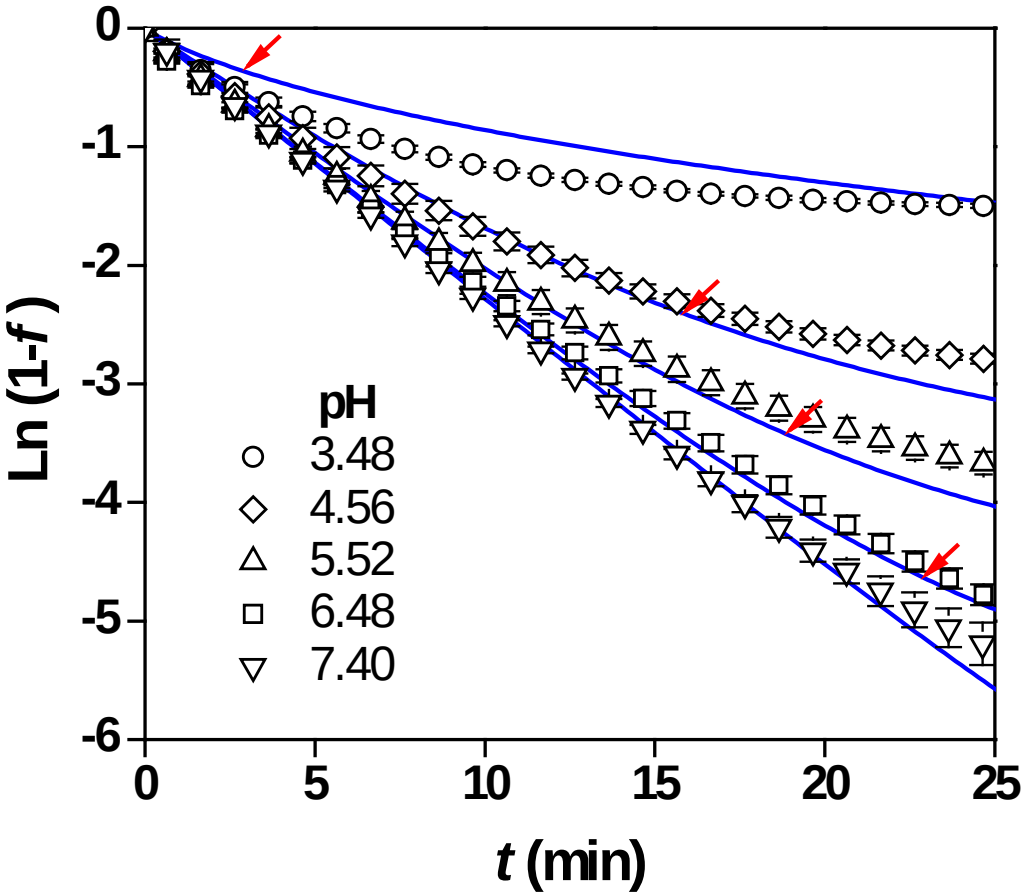

Figure 6. Sorption curves of Cd on Chelex 100 at different pH values (shown in the internal legend). Symbols: experimental data. Lines: MCM predictions using parameter values listed in Table 3 subject to eq. (20) constraint. Experimental conditions: $c_M^*(0)$ *=5×10-5 M (except for pH 7.40, where a concentration of 1.4×10-5 M was used to prevent precipitation), Ionic strength = 0.1M in* $NaNO_3$*,* $m_{dry\ resin}$ *= 24.5 mg. The experiments at pH 6.48 and 7.40 were performed in solutions buffered with 1 mM MOPS. Each experiment was performed in duplicate, and the error bars represent the standard deviation of the measurements. The arrows indicate the points where the predominant transport mechanism changes from external film to internal diffusion (i.e., values of t and f corresponding to equal values of the metal flux according to FDM and IDM).*

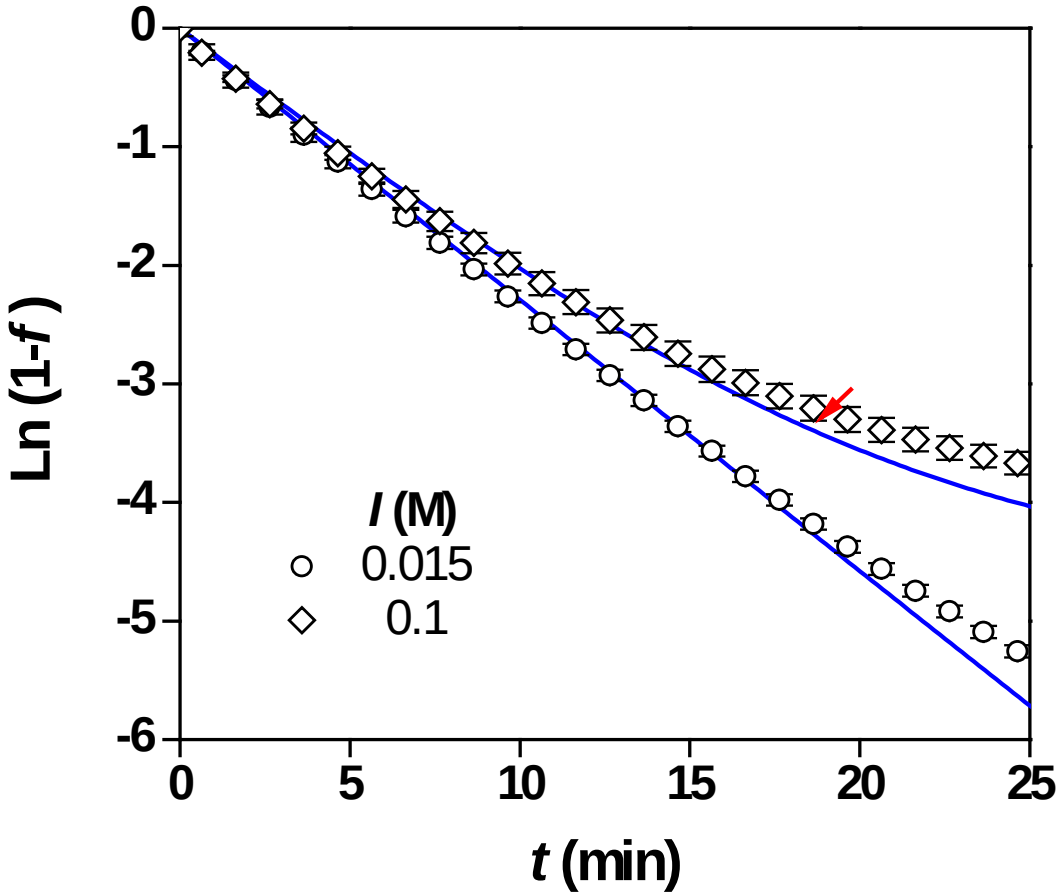

Figure 7. Sorption curves of Cd on Chelex 100 at different ionic strengths (shown in the internal legend). Symbols: experimental data. Lines: model predictions with MCM. Experimental conditions: pH = 5.52; $m_{\text{dry resin}}$ *= 41.1 mg,* $c_{\text{M}}^{*}(0) = 5\times10^{-5}$ *M, background electrolyte:* $NaNO_3$*. The arrow indicates the point where the predominant transport mechanism changes from external film to internal diffusion. At I = 0.0015 M, the transition point lies beyond the timescale of the experiments.*

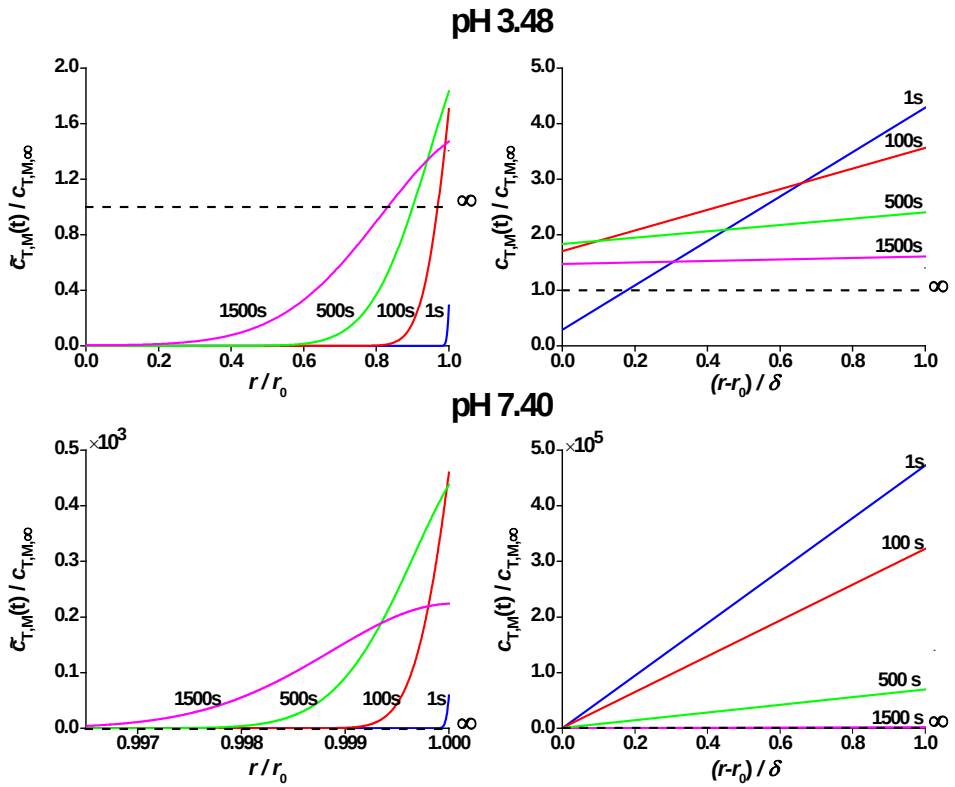

Figure 8. Concentration profiles of Cd in the resin bead (left) and DBL (right) at pH 3.48 (above) and 7.40 (below), calculated using eq. (SI.15) at 1, 100, 500 and 1500 s. The values of the parameters are reported in Table 3. The concentration values are normalised with respect to the local equilibrium concentration, computed from eq. (9) at $t \to \infty$ *(dashed line).*

8. Tables

Table 1 - Values of the parameters used to fit the curves of Fig. 5. All the experiments were carried out with the same mass of dry resin (36.0 mg); the stirring rates correspond to the settings of the OrionStar Series Automatic Stirrer Probe

stirring rate	***I* (M)**	***pH***	***κ***	D_M (m^2/s)	χ	$\tilde{D}$(m^2/s)	V_T (m^3) /10^{-6}	V_R (m^3) /10^{-6}	r_0 (m) /10^{-6}	δ (m) /10^{-6}
1	*0.1*	*7.3*	3.15×10^{8}	7×10^{-10}	6.9	7.67×10^{-18}	50.53	0.108	107	43.5
2	*0.1*	*7.3*	3.15×10^{8}	7×10^{-10}	6.9	7.67×10^{-18}	50.53	0.108	107	24.0
3	*0.1*	*7.3*	3.15×10^{8}	7×10^{-10}	6.9	7.67×10^{-18}	50.54	0.108	107	14.8
4	*0.1*	*7.3*	3.15×10^{8}	7×10^{-10}	6.9	7.67×10^{-18}	50.51	0.108	107	10.3
5	*0.1*	*7.3*	3.15×10^{8}	7×10^{-10}	6.9	7.67×10^{-18}	50.50	0.108	107	7.0

Table 2 – Parameters used to draw the MCM curves of Figs. 6 and 7. All the experiments were carried out with the same mass of dry resin (24.5 mg)

experiment n°	***stirring rate***	***I* (M)**	***pH***	***κ***	D_M (m^2/s)	χ	$\tilde{D}$(m^2/s)	V_T (m^3) /10^{-6}	V_R (m^3) /10^{-6}	r_0 (m) /10^{-6}	δ (m) /10^{-6}
1	5	*0.1*	*3.48*	3.63×10^{3}	7×10^{-10}	3.1	1.34×10^{-13}	50.65	0.046	95	7
2	5	*0.1*	*4.56*	1.21×10^{5}	7×10^{-10}	5.5	1.27×10^{-14}	50.43	0.057	101	7
3	5	*0.1*	*5.52*	5.40×10^{5}	7×10^{-10}	6.8	4.41×10^{-15}	50.46	0.064	104	7
4	5	*0.1*	*6.48*	5.55×10^{6}	7×10^{-10}	6.8	4.26×10^{-16}	50.53	0.069	107	7
5	5	*0.1*	*7.40*	3.45×10^{8}	7×10^{-10}	6.9	6.88×10^{-18}	50.30	0.069	107	7
6	5	*0.0015*	*5.52*	6.46×10^{7}	7×10^{-10}	147.2	1.70×10^{-14}	50.50	0.070	109	7

9. Nomenclature

Bi_{m}	mass transfer Biot number
c_{R}	concentration of binding groups in the resin phase (mol/L)
$\tilde{c}_{\mathrm{T,M}}(r,t)$	total metal concentration in the resin phase (mol/L)
$\tilde{c}_{\mathrm{MR}}(r,t)$	concentration of metal bound to the resin groups (mol/L)
$\tilde{c}_{\mathrm{M,free}}(r,t)$	concentration of free metal inside the resin (mol/L)
$\tilde{c}_{\mathrm{T,M}}(r_0^-,t)$	total metal concentration at the interface inside the bead (mol/L)
$c_{\mathrm{M}}(r_0^+,t)$	metal concentration at the interface outside the bead (mol/L)
$c_{\mathrm{M}}^*(t)$	bulk concentration in the solution (mol/L)
$\tilde{D}$	overall diffusion coefficient in the resin phase (m^2/s)
D_{M}	diffusion coefficient of free metal in water (m^2/s)
$\tilde{D}_{\mathrm{M}}$	diffusion coefficient of free metal in the resin phase (m^2/s)
f	fractional attainment of equilibrium
FDM	Film Diffusion Model
I	ionic strength (mol/L)
IDM	Intraparticle Diffusion Model
J	metal flux through the interface ($mol/m^2/s$)
K_{MR}	stability constant of the metal-resin complex
MCM	Mixed Control Model
r	distance from the centre of the bead (m)
r_0	radius of the bead (m)
r_1	distance from the centre of the bead at which bulk conditions are attained (m)
R_1, R_2, R_3	solutions of eq. (14)

s	variable of the Laplace transform (s^{-1})
t	time (s)
V_R	volume of the resin (m^3)
V_T	total volume (m^3)
w	partition ratio (capacity parameter) $V_R\kappa/(V_T - V_R)$
δ	effective thickness of the DBL (m)
κ	(global) partition coefficient
χ	Donnan partition coefficient